ARID1A restrains EMT and stemness of ovarian cancer cells through the Hippo pathway

SHOUYING XU[1], CHONGYING ZHU[2], QIANG XU[1], ZIHAO AN[1], SHU XU[1], GE XUAN[3], CHAO LIN[4] and CHAO TANG[1]

[1]National Clinical Research Center for Child Health of the Children's Hospital, Zhejiang University School of Medicine, Hangzhou, Zhejiang 310052, P.R. China; [2]The Department of Obstetrics and Gynecology, Ruijin Hospital, Shanghai Jiaotong University School of Medicine, Shanghai 200025, P.R. China; [3]Department of Gynecology, Ningbo Women and Children's Hospital, Ningbo, Zhejiang 315012, P.R. China; [4]Department of Neurosurgery, The Children's Hospital, Zhejiang University School of Medicine, Hangzhou, Zhejiang 310052, P.R. China

Received March 15, 2024; Accepted June 3, 2024

DOI: 10.3892/ijo.2024.5664

Abstract. Genes encoding subunits of SWI/SNF (BAF) chromatin-remodeling complexes are recurrently mutated in a broad array of tumor types, and among the subunits, ARID1A is the most frequent target with mutations. In the present study, it was reported that ARID1A inhibits the epithelial-mesenchymal transition (EMT) and stemness of ovarian cancer cells, accompanied by reduced cell viability, migration and colony formation, suggesting that ARID1A acts as a tumor suppressor in ovarian cancer. Mechanistically, ARID1A exerts its inhibitory effects on ovarian cancer cells by activating the Hippo signaling pathway. Conversely, the overexpression of a gain-of-function transcriptional co-activator with PDZ-binding motif (TAZ) mutant (TAZ-Ser89) effectively reverses the effects induced by ARID1A. In addition, activation of Hippo signaling apparently upregulates ARID1A protein expression, whereas ectopic expression of TAZ-Ser89 results in the markedly decreased ARID1A levels, indicating a feedback of ARID1A-TAZ in regulating ovarian cancer cell EMT and stemness. Thus, the present study uncovered the role of ARID1A through the Hippo/TAZ pathway in modulating EMT and stemness of ovarian cancer cells, and providing with evidence that TAZ inhibitors could effectively prevent initiation and metastasis of ovarian cancer cases where ARID1A is lost or mutated.

Correspondence to: Professor Chao Tang, National Clinical Research Center for Child Health of the Children's Hospital, Zhejiang University School of Medicine, 3333 Binsheng Road, Hangzhou, Zhejiang 310052, P.R. China
E-mail: chtang@zju.edu.cn

Key words: AT-rich interaction domain 1A, Hippo, transcriptional co-activator with PDZ-binding motif, stemness, ovarian cancer

Introduction

Ovarian cancer, one of the most lethal gynecological malignancies, affects 240,000 women worldwide annually, with a five-year survival rate <45% (1). Ovarian cancers can be classified into different types based on clinical behavior, histopathology, and molecular and genetic analyses. These include type I (low-grade serous carcinomas, low-grade endometrioid carcinomas, clear cell carcinomas and sero-mucinous carcinomas) and type II (high-grade serous carcinomas, high-grade endometrioid carcinomas and undifferentiated carcinomas) tumors, with epithelial ovarian malignancies accounting for the majority (2). Previous epidemiological studies and meta-analyses have identified several risk factors for ovarian cancer, including family genetic history (for example, mutations in BRCA1 and BRCA2 genes), contraceptive use, short lactation duration, a body mass index ≥30 kg/m^2, and other gynecological diseases such as vaginitis and polycystic ovary syndrome (1,3).

Curative and survival trends in ovarian cancer have not significantly improved owing to the challenges of early diagnosis, including the lack of clear screening tools, and indistinct signs and symptoms. Moreover, high metastasis and recurrence rates and drug resistance to chemotherapy are also important reasons for the poor prognosis of patients with ovarian cancer (4). Therefore, it is important to identify potential ovarian cancer targets and clarify their roles and molecular mechanisms in the malignant biological behavior of ovarian cancer.

Cancer stem cells (CSCs), a subpopulation within tumors, possess self-renewal and differentiation capacities akin to those of stem cells, thus sustaining tumor growth and the regeneration of an heterogeneous tumor mass (5,6). Accumulating evidence indicates that CSCs exist in numerous types of tumors, including leukemia, breast, rectal and ovarian cancer. A previous study revealed that CSCs have become the significant drivers of chemoresistance in ovarian cancer (7). Hu *et al* (8) in 2010 also found that the CSCs residing in ovarian epithelial tumors are not targeted by chemotherapy, which is the primary cause of chemotherapy failure. Therefore,

a therapeutic approach is required to eliminate rapidly proliferating differentiated cancer cells and slow-proliferating drug-resistant CSCs. The generation of CSCs is highly regulated by the molecular process of epithelial-mesenchymal transition (EMT), which plays a key role in the growth and metastasis of tumors (9,10), Therefore, determining the key mediators participating in the regulation of CSC function, such as EMT, could provide a potential therapeutic target for the treatment of ovarian cancer metastasis.

The Hippo signaling pathway controls tissue growth and cell fate, and the dysregulation of Hippo activity leads to the development of tumors, including ovarian cancer. In mammals, the core components of the Hippo pathway are a pair of related serine/threonine kinases, including mammalian STE20-like protein kinase 1 (MST1) and 2 (MST2) and the large tumor suppressor kinases (LATS1/2) (11). Activation of Hippo signaling restricts tissue growth by promoting LATS1/2-dependent phosphorylation of the homologous oncoproteins, including Yes-associated protein (YAP) and transcriptional co-activator with PDZ-binding motif (TAZ). The phosphorylated (p-) YAP and TAZ accumulate in the cytoplasm, where they are degraded by ubiquitination-dependent proteasome (12). By contrast, the inhibition of Hippo signaling results in tissue growth and cell viability via YAP and TAZ, which translocate to the nucleus to transactivate targets in cooperation with the TEAD transcription factor.

As a member of the SWItch/Sucrose Non-Fermenting (SWI/SNF) chromatin remodeling complex, AT-rich binding domain 1A (ARID1A) uses the energy of ATP hydroxylation to reshape the chromatin structure and can slide nucleosomes along the DNA template (13). Abnormal ARID1A expression occurs at a high frequency in congenital conditions and various cancers, including ovarian cancer (14,15). ARID1A participates in regulating the expression of various target genes in nucleus, whose alteration gives rise to tumor progression. For example, in bladder cancer, co-mutations in the ARID1A, GPRC5A and MLL2 genes enhance the self-renewal and tumorigenesis of bladder cancer non-stem cells, which contribute to the characteristics of cancer cell stemness (16), suggesting the role of ARID1A as a stemness mediator in cancer cells.

Different from the previous findings that ARID1A commonly functions by affecting gene expression in nucleus, in the present study, it was reported that ARID1A inhibits EMT and stemness in ovarian cancer cells by participating in the regulation of Hippo signaling activity, with the downregulated cell viability, migration and colony formation. This suggests that ARID1A functions as a tumor suppressor in ovarian cancer. In addition, the current data exhibited that Hippo activity reciprocally exerts effects on ARID1A expression, indicating a feedback regulation between Hippo and ARID1A in ovarian cancer cells. Thus, ARID1A could be a novel prognostic molecule for ovarian cancer and a potential target for drug development for the treatment of ovarian cancer.

Materials and methods

Cell lines and cell culture. Human ovarian cancer cell lines SK-OV-3 and A2780 and 293T cells were obtained from the American Type Culture Collection (ATCC), and were maintained in high glucose DMEM (Thermo Fisher Scientific, Inc.) supplemented with 10% (v/v) fetal bovine serum (FBS; Thermo Fisher Scientific, Inc.) and 1% (v/v) penicillin/streptomycin (Beyotime Institute of Biotechnology) as previously described (17-19). All the cells were cultured at 37˚C in a humidified chamber with 5% CO_2.

Generation of SK-OV-3-derived ovarian cancer stem-like cells (OCSCs). The SK-OV-3 derived OCSCs were generated as previously described (20). Briefly, SK-OV-3 cells were harvested and washed with FBS-free DMEM medium twice, then re-suspended and maintained under stem cell conditions by serum-free in DMEM medium supplemented with 5 mg/ml insulin (Sigma-Aldrich; Merck KGaA), 10 ng/ml human recombinant epidermal growth factor (Invitrogen; Thermo Fisher Scientific, Inc.), 10 ng/ml basic fibroblast growth factor (Invitrogen; Thermo Fisher Scientific, Inc.) and 0.3% bovine serum albumin (Sigma-Aldrich; Merck KGaA). Culture media were changed every 2 days by centrifuging the cells at 60 x g for 5 min at room temperature to remove the dead cell debris and SK-OV-3 cells proliferated as non-adherent spheres consequently in this condition. The cells of non-adherent spheres were subjected to identification of stem cell-like properties before following experiments.

Antibodies and reagents. Antibodies for ARID1A (mouse; cat. no. sc-32761), YAP (cat. no. sc-101199), CTGF (cat. no. sc-373936), CYR61 (cat. no. sc-374129), Nanog (cat. no. sc-293121), Sox2 (cat. no. sc-365823), Oct3/4 (cat. no. sc-5279), GAPDH (cat. no. sc-32233) and normal mouse IgG (cat. no. sc-2025) were purchased from Santa Cruz Biotechnology, Inc. Antibodies for p-YAP antibody (cat. no. AF5965), α-Tubulin (cat. no. AF0001), N-cadherin (cat. no. AF5237) and E-cadherin (cat. no. AF0138) were obtained from Beyotime Institute of Biotechnology. p-MST1 (cat. no. bs-3294R), MST1 (cat. no. bs-3504R), p-LATS1 (cat. no. bs-3245R), LATS1 (cat. no. bs-2904R), TAZ (cat. no. bs-12367R) and Vimentin (cat. no. bs-23063R) antibodies were purchased from BIOSS. Normal rabbit IgG (cat. no. 2729) and p-TAZ antibody (cat. no. 59971) were obtained from Cell Signaling Technology, Inc.

Short hairpin RNA (shRNA) sequences, viruses and infection. Plasmids expressing ARID1A-shRNA were generated by insertion with the hairpin shRNA templates of complementary oligonucleotides at the sites of XbaI and NotI into the shRNA expression vector, Pll3.7. ShRNA sequences used are as follows: shRNA sequence targeting ARID1A: 5'-AAC CAAAGTTACTGTTGTTTA-3'; and a scrambled shRNA sequence (5'-TTTGTACTACACAAAAGTACTG-3') was used as control. Sequences were obtained from Shanghai Sangon Biotechnology Co. Ltd. Lentiviruses expressing ARID1A-shRNA or scrambled-shRNA were generated by co-transfecting the HEK293T packaging cells with lentiviral shRNA expression vector, and lentiviruses-containing supernatants with the titers greater than $1x10^6$ cfu/ml was used for infection of cells in the presence of 8 μg/ml polybrene (Sigma-Aldrich; Merck KGaA) as previously described (21).

Transfection. Transient transfection was performed using Lipofectamine 2000 reagent (Invitrogen; Thermo Fisher

Scientific, Inc.) with Opti-MEM (cat. no, 31985-062; Invitrogen; Thermo Fisher Scientific, Inc.) medium according to the manufacturer's instructions. Briefly, SK-OV-3 or A2780 cells were transfected with 10 μg indicated plasmids. At 12 h after transfection, the cells were cultured in fresh medium, and the cells were collected 48 h after transfection. Then the cellular lysates were subjected to reverse transcription-quantitative PCR (RT-qPCR), western blotting (WB) or other assays.

RNA isolation and RT-qPCR. Total RNA was extracted from SK-OV-3 cells and A2780 cells by using a TRIzol reagent (Takara Biotechnology Co., Ltd.) according to the manufacturer's instructions. 5 μg of total RNA was reversely transcribed by using SuperScript III reagent (Thermo Fisher Scientific, Inc.) according to the manufacturer's protocol, and the oligo-(deoxythymidine) primer with incubation at 42˚C for 1 h. After the termination of cDNA synthesis, mRNA levels of target genes were determined by RT-qPCR as previously described (21). Briefly, the initial denaturation was 95˚C for 5 min; followed by 40 cycles of denaturation (95˚C, 10 sec), annealing and extension (60˚C, 30 sec). All reactions were conducted in a 20 μl reaction volume in triplicate. The relative expression of the mRNA levels was normalized to the GAPDH levels, and the relative difference in mRNA levels was calculated by the $2^{-\Delta\Delta Cq}$ method (22). The primers used were as follows: ARID1A forward, 5'-TCATGCCCAACCTTC GTATC-3' and reverse, 5'-GATGGCTGCTGGGAGTATG-3'; CTGF forward, 5'-CCTGTGCAGCATGGACGTT-3' and reverse, 5'-GGACCAGGCAGTTGGCTCTAA-3'; CYR61 forward, 5'-CTCCCTGTTTTTGGAATGGA-3' and reverse, 5'-TGGTCTTGCTGCATTTCTTG-3'; Nanog forward, 5'-CCATCCTTGCAAATGTCTTCTG-3' and reverse, 5'-CTT TGGGACTGGTGGAAGAATC-3'; Sox2 forward, 5'-GTG GTTACCTCTTCCTCCCACT-3' and reverse, 5'-AGTGCT GGGACATGTGAAGTCT-3'; Oct3/4 forward, 5'-GTGGAG GAAGCTGACAACAATG-3' and reverse, 5'-AATTCTCCA GGTTGCCTCTCACT-3'; E-Cadherin forward, 5'-ACCAAC GATAATCCTCCGAT-3' and reverse, 5'-TCAGTGTGGTGA TTACGACG-3'; N-Cadherin forward, 5'-AATCCTCCA GAGTTTACTGC-3' and reverse, 5'-TCCTTATCGGTCACA GTTAG-3'; Vimentin forward, 5'-GAGAGGAAGCCGAAA ACAC-3' and reverse, 5'-TGCGTTCAAGGTCAAGACG-3'; and GAPDH forward, 5'-CCTGTTCGACAGTCAGCCG-3' and reverse, 5'-CGACCAAATCCGTTGACTCC-3'.

WB. WB was performed using standard protocols as previously described (23). Briefly, cells were harvested and rinsed with pre-chilled PBS on ice, and then cell lysates were prepared using RIPA buffer (Beyotime Institute of Biotechnology). BCA protein assay kit was conducted to detect the concentration of protein. Generally, 50 μg of total protein was subjected to 8-15% sodium dodecyl sulfate polyacrylamide gel electrophoresis (SDS-PAGE) and transferred onto PVDF membrane (MilliporeSigma). Membranes were then blocked with 5% non-fat milk at room temperature for 1 h followed by incubation with different primary antibodies (1:1,000) at 4˚C overnight. The membranes were then incubated with corresponding HRP-labeled Goat Anti-Rabbit IgG (H + L) (1:1,000 cat. no. A0208˝ Beyotime Institute of Biotechnology) for 1 h at room temperature the following day. Signals were subsequently detected using an ECL Kit (cat. no. P0018AS; Beyotime Institute of Biotechnology) according to the manufacturer's protocol.

Immunoprecipitation. SK-OV-3 or A2780 cells were washed with PBS and lysed with ice-cold extraction buffer (1% Triton-X 100, 10 mM EDTA, 1 mM PMSF, 1% Cocktail, pH=7.4). The soluble fraction was obtained by centrifuging cell lysates at 13,523 x g for 10 min at 4˚C. The prepared supernatants were incubated at 4˚C overnight with an ARID1A antibody, a TAZ antibody or control IgG. Then the mixture was incubated with 50 μl protein-A-agarose beads (Beyotime Institute of Biotechnology) for 2 h at 4˚C, followed by three times of washing using lysis buffer. Immunoprecipitants were eluted with SDS loading buffer and resolved in SDS-PAGE gels. The proteins were transferred onto PVDF membranes and were further probed with appropriate antibodies correspondingly, referring to the a forementioned method in WB.

Cell Counting Kit-8 (CCK-8) assay. CCK-8 assay was performed as per the manufacturer's instructions (Shanghai Yeasen Biotechnology Co., Ltd.) as previously described (24). Briefly, 24 h after transfection, cells were seeded into 96-well plates at a cell density of ~$4x10^3$ cells/well. At the selected time course after attachment, cells were incubated with 10 μl CCK-8 reagent for 2 h in the dark at 37˚C, and optical density was consequently measured at a wavelength of 450 nm using a microplate reader (Tecan Group, Ltd.).

Wound healing assay. Wound healing assay was performed as previously described (15). Briefly, SK-OV-3 cells were seeded in six-well plate at $2x10^5$ cells/well and cultured for 24 h to confluence. Subsequently, cells were incubated with serum-free medium for 12 h. A sterile tip was used to scratch a straight line in each well. Then the wound gaps were monitored by light microscopy after 24 h, and were calculated using ImageJ software (National Institutes of Health). Experiments were performed for three independent experiments.

Colony formation assay. The colony formation assay was performed as previously described (23). A cell colony formed by the offspring of a single cell for >6 consecutive generations *in vitro* is called a colony, containing >50 cells. Briefly, SK-OV-3 cells were placed into a six-well plate at a density of ~500 cells/well, and were cultured at 37˚C for two weeks. Colonies were then fixed with 4% paraformaldehyde (PFA) for 15 min and stained with 0.5% crystal violet (Sigma-Aldrich; Merck KGaA) in 2% ethanol for 10 min. After rinsing and drying, colonies were counted manually and images were captured. Each experiment was performed in triplicate.

Xenograft assay. Animal experiments were approved (approval no. 21045) by the Animal Ethics Committee of Zhejiang University (Zhejiang, China) and performed according to the Guide for the Care and Use of Laboratory Animals (NIH Publication no. 85-23, revised 1996). A total of 10 BALB/c nude mice (age, 4-5 weeks; weight, 18-20 g) were purchased from Vital River Laboratory Animal Technology Co., Ltd. and were bred under pathogen-free conditions (temperature, 18-22˚C; humidity, 50-60%; 12/12-h light/dark cycle). The

mice bedding, feed and water were replaced every 2 days. Mice were allocated into two groups: Control group and ARID1A group (n=5 in each group). Stably ARID1A-expressing viruses-infected (ARID1A) or control viruses-infected (Control) SK-OV-3 cells ($1x10^6$ cells in 100 μl PBS) were injected into the right flank of mice ($5x10^6$ cells per mouse) via subcutaneous injection. The volumes (V) of the xenograft tumors were examined every 3 days as follows: $V=0.5 x a x b^2$, where 'a' indicates the long axis and 'b' indicates the short axis. After 21 days, the mice began to succumb and were immobile and rigid, and were not in a favorable mental state, the body weight was very low, and certain tumors reached the 1-1.5 cm in diameter. To reduce suffering, the mice were euthanized via intraperitoneal injection of 120 mg/kg pentobarbital sodium. Verification of death included cardiac and respiratory arrest, lack of reflexes and changes in mucosal color. The subcutaneous tumor tissues were consequently dissected and collected, and were weighed and used for subsequent examinations.

Immunohistochemistry for Ki67. The collected xenograft tumor tissues were fixed in 4% PFA, embedded in paraffin, cut into sections with the thickness of 4 μm, dewaxed with xylene (Sinopharm Chemical Reagent Co., Ltd.) and rehydrated (100% ethanol for 3 min, 95% ethanol for 2 min, 80% ethanol for 2 min, 75% ethanol for 2 min, H_2O for 1 min). Then, the sections were treated with 0.01 M citrate buffer for antigen retrieval, incubated with 3% H_2O_2 solution at room temperature for 10 min, and incubated with 5% goat serum (Beyotime Institute of Biotechnology) at 37˚C for 30 min. Next, the sections were incubated with the primary antibody against Ki67 (1:100; cat. no. ER1706-46; HUABIO) at 4˚C overnight, and then with goat anti-rabbit IgG H&L (HRP) secondary antibody diluted at 1:1,000 at room temperature for 30 min next day. After DAB and hematoxylin staining, the sections were sealed with neutral resin and observed under a light microscope.

Statistical analysis. The results are presented as the mean ± SD. The SPSS 19.0 software program (IBM Corp.) and Excel (Excel 2016; Microsoft Corporation) were used for statistical analysis. Statistical significance of the data was analyzed by unpaired Student's t-test between two groups or with one-way ANOVA among multiple groups, followed by Dunnett's post hoc test. All P-values were two-sided, and $P<0.05$ was considered to indicate a statistically significant difference. All the experiments were repeated for a minimum of three times independently.

Results

ARID1A regulates EMT and stemness in ovarian cancer cells. To explore the role of ARID1A in ovarian cancer cells, the ovarian cancer cell line SK-OV-3 was transfected with an ARID1A-expressing vector to ectopically express ARID1A and a vector expressing ARID1A-shRNA to suppress endogenous ARID1A expression. The results revealed that ARID1A overexpression significantly inhibited SK-OV-3 cell viability (Fig. 1A), whereas silencing ARID1A increased SK-OV-3 cell viability (Fig. 1B). Moreover, ARID1A overexpression suppressed SK-OV-3 cell migration and decreased colony numbers (Fig. 1C, D, G and H), whereas ARID1A knockdown significantly enhanced the migratory and colony formation abilities of SK-OV-3 cells (Fig. 1E, F, I and J). Consistent with these results, ARID1A-overexpression increased the expression of epithelial markers such as E-cadherin and decreased the expression of mesenchymal markers (including N-Cadherin and Vimentin), and stemness markers (such as Nanog, Oct3/4 and Sox2) (Fig. 1K and L). ARID1A knockdown resulted in the opposite effects (Fig. 1M and N), illustrating that ARID1A regulates EMT and stemness in ovarian cancer cells.

ARID1A controls Hippo signaling activity in ovarian cancer cells. The Hippo pathway is closely associated with EMT and stemness in cancer cells (7,25). The potential effect of ARID1A on Hippo signaling was investigated to gain insight into the molecular mechanism connecting ARID1A expression with EMT and stemness in ovarian cancer cells. The protein levels and phosphorylation status of the main components of the Hippo pathway (MST1/2, LATS1/2, TAZ and YAP) (26) were analyzed in ovarian cancer cell lines expressing ARID1A or ARID1A-shRNA. The present results revealed that ARID1A overexpression resulted in a more active Hippo pathway in SK-OV-3 ovarian cancer cells, with an increased ratio of p-MST1/total MST1 and p-LATS1/total LATS1, compared with that in the control (Fig. 2A). Conversely, ARID1A-shRNA-expressing SK-OV-3 cells displayed a less active Hippo pathway with a decreased p-MST1/total MST1 to p-LATS1/total LATS1 ratio compared with the control cells (Fig. 2B). Consistent with this, p-TAZ and p-YAP levels were upregulated, but total TAZ and YAP expression was downregulated upon ARID1A-overexpression (Fig. 2C), whereas suppression of ARID1A expression by ARID1A-shRNA exerted the opposite effects (Fig. 2D). As expected, the mRNA and protein expression of TAZ/YAP-mediated target genes, including CTGF and CYR61, was significantly reduced by ARID1A overexpression and induced by ARID1A knockdown (Fig. 2E-H). This result was verified using the human ovarian cancer A2780 cell line, demonstrating that ARID1A affected CTGF and CYR61 mRNA expression (Fig. 2I and J). Thus, Hippo signaling activity was revealed to be regulated by ARID1A in ovarian cancer cells.

Hippo activation induces ARID1A expression and inhibits EMT and stemness in ovarian cancer cells. Cell density mediates Hippo pathway activity in cultured cells (27). To test the possible reciprocal effect of Hippo activity on ARID1A expression, SK-OV-3 cells were seeded at either low or high densities to deactivate or activate the Hippo pathway, respectively, which was estimated by examining the target gene CTGF and CYR61 expression (Fig. 3A). Activation of Hippo signaling by high cell density upregulated ARID1A protein expression (Fig. 3B), whereas ARID1A mRNA levels remained unchanged (Fig. 3B), suggesting that Hippo regulates ARID1A at a translational or post-translational level. As expected, activation of the Hippo pathway at high density weakened EMT and stemness in SK-OV-3 cells. This was associated with upregulated E-cadherin expression and downregulated expression of N-cadherin, Vimentin (Fig. 3C) and stemness markers (Nanog, Oct3/4 and Sox2) at both the mRNA and

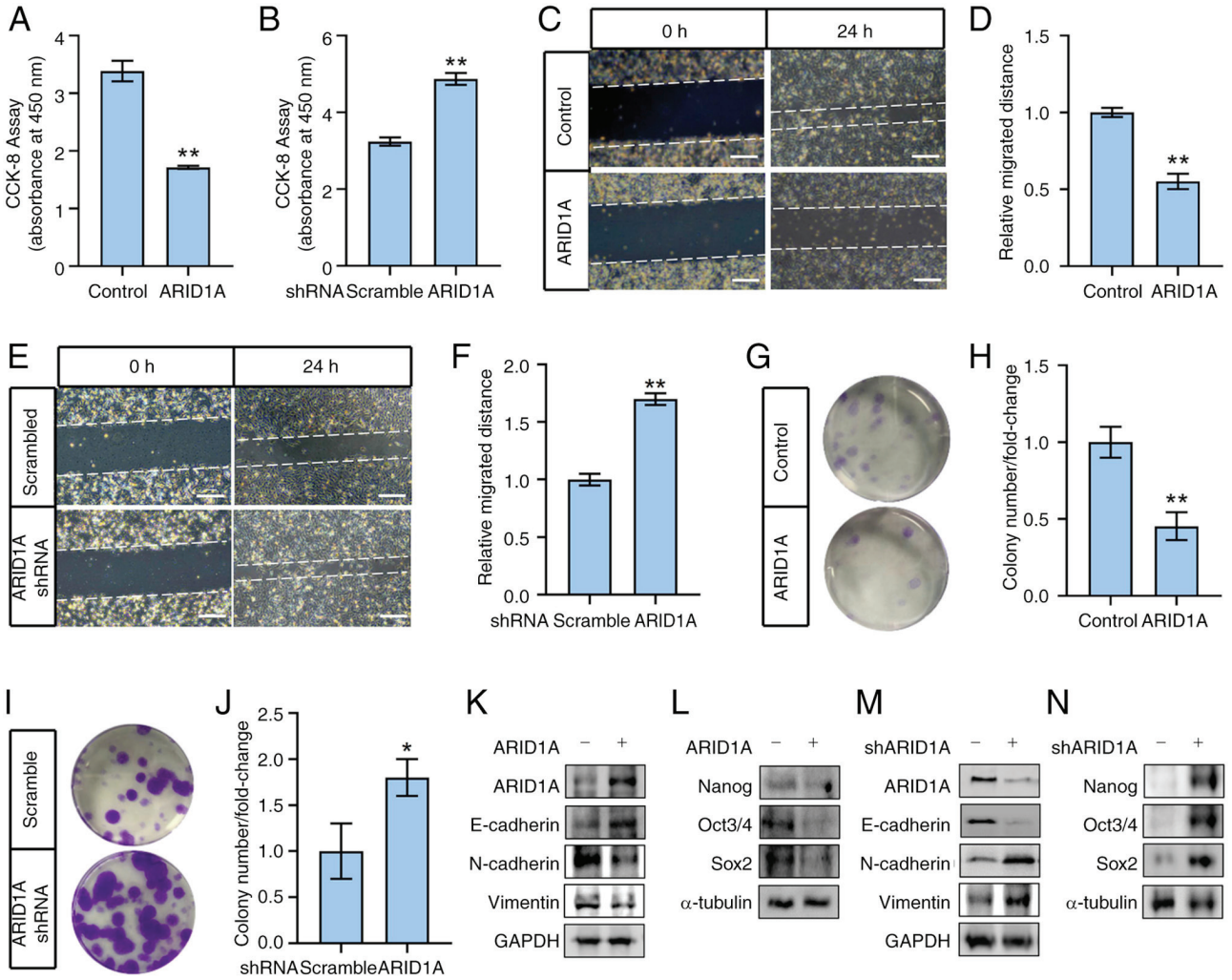

Figure 1. ARID1A regulates epithelial-mesenchymal transition and stemness in ovarian cancer cells. (A) SK-OV-3 cells were transfected with ARID1A-overexpressing or control vector (Control) and cell viability was measured after 48 h by CCK-8 assay. (B) SK-OV-3 cells were transfected with ARID1A-shRNA or control shRNA (Scramble) and cell viability was measured after 72 h by CCK-8 assay. (C) SK-OV-3 cells were transfected with ARID1A-overexpressing or control vector (Control) and cell migration was measured at 24 h after scratch by wound healing assay. (D) Quantitative statistics of panel C. (E) SK-OV-3 cells were transfected with ARID1A-shRNA or control shRNA (Scramble) and cell migration was measured at 24 h after scratch by wound healing assay. (F) Quantitative statistics of panel E. (G) SK-OV-3 cells were transfected with ARID1A-overexpressing or control vector (Control) and cell colony formation assay was performed. (H) Quantitative statistics of panel G. (I) SK-OV-3 cells were transfected with ARID1A-shRNA or control shRNA (Scramble) and cell colony formation assay was performed. (J) Quantitative statistics of panel I. (K) SK-OV-3 cells were transfected with ARID1A-overexpressing (ARID1A$^+$) or control vector (ARID1A-) and protein levels of ARID1A, E-Cadherin, N-Cadherin and Vimentin were measured by WB after 48 h. GAPDH was used as loading control. (L) SK-OV-3 cells were transfected with ARID1A-overexpressing (ARID1A$^+$) or control vector (ARID1A$^-$) and protein levels of Nanog, Oct3/4 and Sox2 were measured by WB after 48 h. α-tubulin was used as loading control. (M) SK-OV-3 cells were transfected with ARID1A-shRNA (shARID1A$^+$) or control shRNA (shARID1A-) and protein levels of ARID1A, E-Cadherin, N-Cadherin and Vimentin were measured by WB after 72 h. GAPDH was used as loading control. (N) SK-OV-3 cells were transfected with ARID1A-shRNA (shARID1A$^+$) or control shRNA (shARID1A-) and protein levels of Nanog, Oct3/4 and Sox2 were measured by WB after 72 h. α-tubulin was used as loading control. Scale bars in C and E, 50 μm. *P<0.05 and **P<0.01 (n=3). ARID1A, AT-rich binding domain 1A; CCK-8 Cell Counting Kit-8; shRNA, short hairpin RNA; WB, western blotting.

protein levels (Fig. 3D and E). By contrast, overexpression of TAZ, a key effector of the Hippo pathway, apparently reduced ARID1A protein expression (Fig. 3F) despite a slight alteration at the mRNA level (data not shown). At a culture condition with medium cell density, the TAZ-overexpressing ovarian cancer cells displayed upregulated EMT and stemness, including decreased E-cadherin expression and increased expression of N-Cadherin and Vimentin (Fig. 3F) and of stemness markers, including Nanog, Oct3/4 and Sox2 (Fig. 3G). Co-immunoprecipitation assays were performed to validate the possible regulation of ARID1A protein expression by Hippo. The present results showed an interaction between endogenous ARID1A and TAZ in SK-OV-3 cells, which could be verified using an ARID1A- or TAZ-antibody in A2780 cells (Fig. 3H-J), suggesting the potential mediation of ARID1A by TAZ. These results indicated that activation of Hippo signaling induces ARID1A expression and suppresses EMT and stemness via TAZ inhibition in ovarian cancer cells.

ARID1A inhibits EMT and stemness by activating the Hippo pathway in ovarian cancer cells. Given that ARID1A negatively regulates EMT and stemness in ovarian cancer cells but positively mediates the Hippo pathway, it was hypothesized that ARID1A affects EMT and stemness in ovarian cancer cells through the Hippo pathway. ARID1A overexpression significantly reduced TAZ-mediated viability, migration and

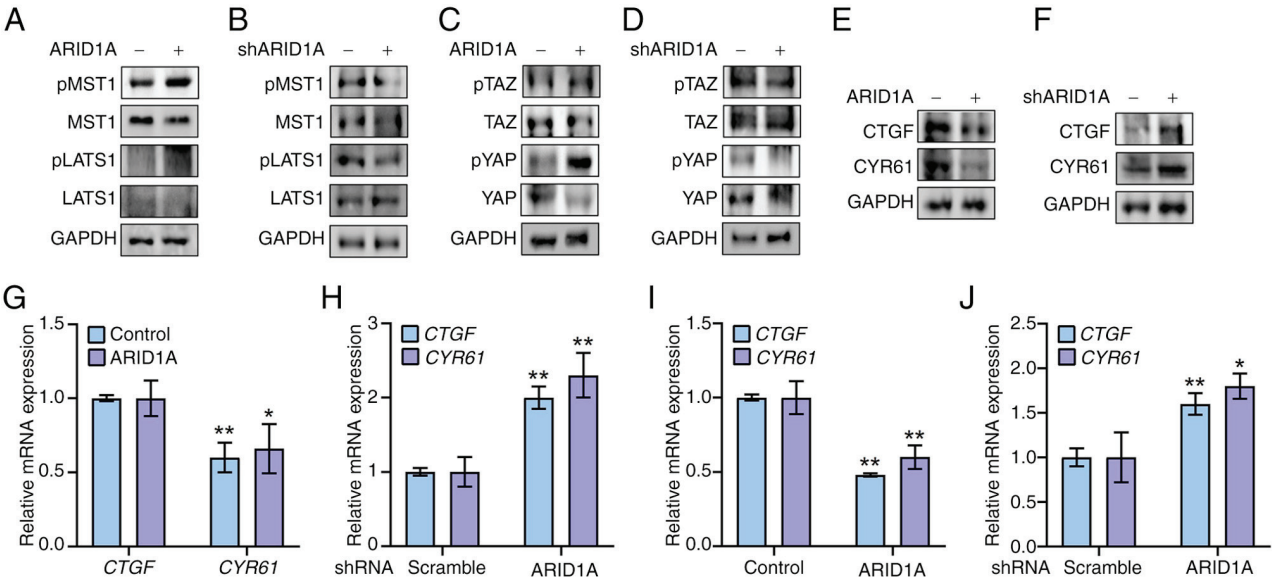

Figure 2. ARID1A controls Hippo signaling activity in ovarian cancer cells. (A) SK-OV-3 cells were transfected with ARID1A-overexpressing (ARID1A$^+$) or control vector (ARID1A$^-$) and protein levels of pMST1, MST1, pLATS1 and LATS1 were measured by WB after 12 h. GAPDH was used as loading control. (B) SK-OV-3 cells were transfected with ARID1A-shRNA (shARID1A$^+$) or control shRNA (shARID1A$^-$) and protein levels of pMST1, MST1, pLATS1 and LATS1 were measured by WB after 24 h. GAPDH was used as loading control. (C) SK-OV-3 cells were transfected with ARID1A-overexpressing (ARID1A$^+$) or control vector (ARID1A-) and protein levels of p-TAZ, TAZ, p-YAP and YAP were measured by WB after 12 h. GAPDH was used as loading control. (D) SK-OV-3 cells were transfected with ARID1A-shRNA (shARID1A$^+$) or control shRNA (shARID1A$^-$) and protein levels of pTAZ, TAZ, pYAP and YAP were measured by WB after 24 h. GAPDH was used as loading control. (E) SK-OV-3 cells were transfected with ARID1A-overexpressing (ARID1A$^+$) or control vector (ARID1A$^-$) and protein levels of CTGF and CYR61 were measured by WB after 12 h. GAPDH was used as loading control. (F) SK-OV-3 cells were transfected with ARID1A-shRNA (shARID1A$^+$) or control shRNA (shARID1A-) and protein levels of CTGF and CYR61 were measured by WB after 24 h. GAPDH was used as loading control. (G) SK-OV-3 cells were transfected with ARID1A-overexpressing (ARID1A) or control vector (Control) and mRNA levels of CTGF and CYR61 were measured by RT-qPCR. (H) SK-OV-3 cells were transfected with ARID1A-shRNA or control shRNA (Scramble) and mRNA levels of CTGF and CYR61 were measured by RT-qPCR. (I) A2780 cells were transfected with ARID1A-overexpressing (ARID1A) or control vector (Control) and mRNA levels of CTGF and CYR61 were measured by RT-qPCR. (J) A2780 cells were transfected with ARID1A-shRNA or control shRNA (Scramble) and mRNA levels of CTGF and CYR61 were measured by RT-qPCR. *P<0.05 and **P<0.01 (n=3). ARID1A, AT-rich binding domain 1A; p-, phosphorylated; shRNA, short hairpin RNA; TAZ, transcriptional co-activator with PDZ-binding motif; RT-qPCR, reverse transcription-quantitative PCR; WB, western blotting.

colony formation in SK-OV-3 cells (Fig. 4A-E). Furthermore, overexpression of a gain-of-function mutant of TAZ (TAZ-S89) effectively countered the effects derived from ARID1A in ovarian cancer cells. This mutant has a mutation at Ser 89 (to Ala), rendering it resistant to phosphorylation by the upstream kinase LATS, and consequently, TAZ-S89 stably enters the nucleus and transactivates the downstream targets (28). The current data revealed that TAZ-S89 not only effectively reversed the ARID1A-suppressd cell viability (Fig. 4F) but mitigated the expression alterations of EMT and stemness markers induced by ARID1A overexpression, including the downregulation of E-cadherin and the upregulation of N-cadherin, Vimentin, Nanog, Oct3/4 and Sox2, compared with cells overexpressing ARID1A alone (Fig. 4G and H). Thus, activation of TAZ could attenuate the ARID1A-trigged suppression of EMT and stemness, reinforcing the notion that ARID1A negatively regulates EMT and stemness by activating the Hippo pathway.

ARID1A-overexpressing OCSCs exhibit less stemness in vitro and in vivo. SK-OV-3-derived OCSCs were isolated to further test the role of ARID1A in ovarian cancer stemness, as previously described (20). The isolated and cultured OCSCs displayed sphere-forming and stem cell-like phenotypes (Fig. 5A). The OCSCs possessed higher viability (Fig. 5B) and exhibited increased mRNA and protein expression of stemness markers Nanog, Oct3/4 and Sox2 (Fig. 5C and D), compared with the parent SK-OV-3 cells. By contrast, ARID1A expression was reduced in the OCSCs (Fig. 5E). However, overexpression of ARID1A in the OCSCs significantly downregulated the mRNA and protein expression of CTGF and CYR61 (Fig. 5F and G). It also lowered the EMT ability and stemness as determined by measuring the expression of E-cadherin, N-cadherin, Vimentin, and stemness markers Nanog, Oct3/4 and Sox2 (Fig. 5H and I). By contrast and as expected, ARID1A overexpression reduced OCSC migration and colony numbers (Fig. 5J-M).

Finally, ARID1A expression was determined by ARID1A-expressing lentiviruses in OCSCs (ARID1A-OCSCs), which were subsequently injected into nude mice to form OCSCs-derived xenografts, to evaluate the roles of ARID1A in OCSCs' stemness *in vivo*. The volumes of control OCSCs and ARID1A-OCSC xenografts increased in a time-dependent manner within 21 days post-inoculation (Fig. 5N). However, no significant difference was observed between the body weights of mice bearing different xenografts (data not shown). Notably, the volumes of xenografts derived from control OCSCs were significantly higher than those of ARID1A-OCSCs from 15 to 21 days post-inoculation (Fig. 5N and O), and the xenograft-derived control OCSCs

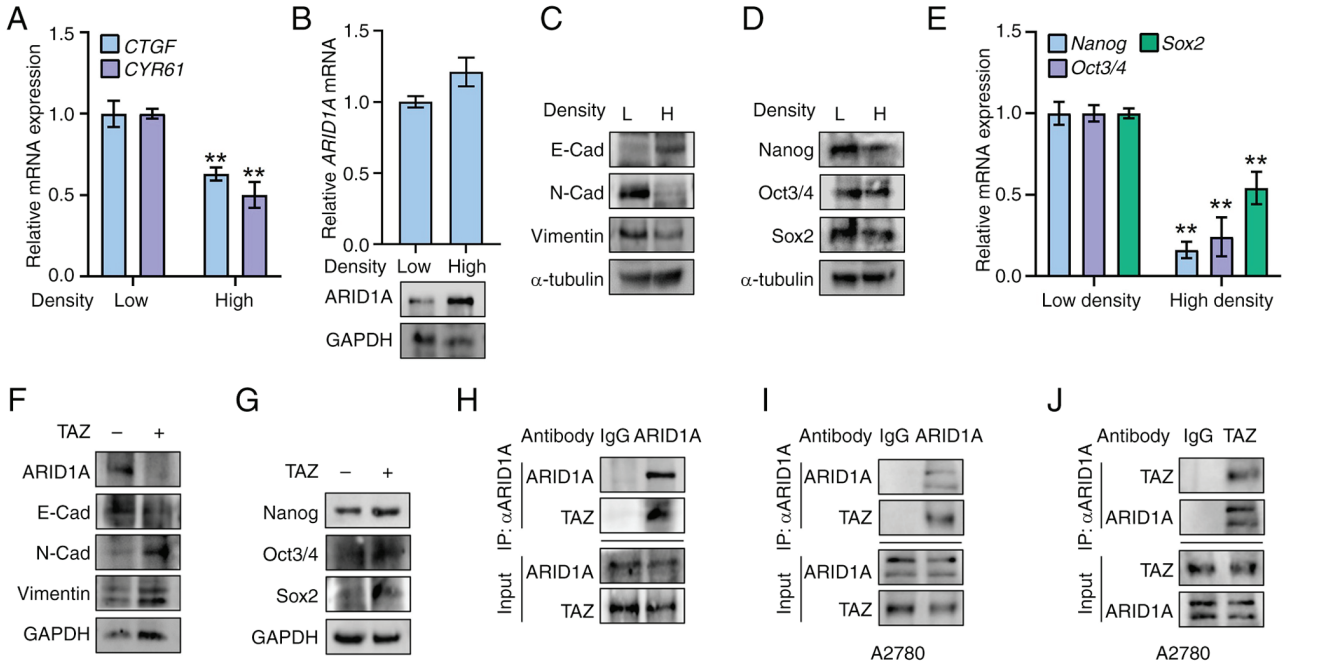

Figure 3. Hippo activation induces ARID1A expression and inhibits epithelial-mesenchymal transition and stemness in ovarian cancer cells. (A) SK-OV-3 cells were cultured in low density (Low) or high density (High) and mRNA levels of CTGF and CYR61 were measured by RT-qPCR. (B) SK-OV-3 cells were cultured in low density (Low) or high density (High) and mRNA levels and protein of ARID1A were measured by RT-qPCR and WB, respectively. (C) SK-OV-3 cells were cultured in low density (L) or high density (H) and protein levels of E-Cadherin, N-Cadherin and Vimentin were measured by WB. α-tubulin was used as loading control. (D) SK-OV-3 cells were cultured in low density (L) or high density (H) and protein levels of Nanog, Oct3/4 and Sox2 were measured by WB. α-tubulin was used as loading control. (E) SK-OV-3 cells were cultured in low density or high density and mRNA levels of Nanog, Oct3/4 and Sox2 were measured by RT-qPCR. (F) SK-OV-3 cells were seeded at a density of $5x10^6$ cells in a 100-mm cell culture dish and were transfected with TAZ-expressing plasmid (TAZ^+) or control vector (TAZ^-). Protein levels of ARID1A, E-Cadherin, N-Cadherin and Vimentin were measured by WB. GAPDH was used as loading control. (G) SK-OV-3 cells were seeded at a density of $5x10^6$ cells in a 100-mm cell culture dish and were transfected with TAZ-expressing plasmid (TAZ^+) or control vector (TAZ^-). Protein levels of Nanog, Oct3/4 and Sox2 were measured by WB. GAPDH was used as loading control. (H) Co-immunoprecipitation of endogenous TAZ and ARID1A in SK-OV-3 cells. IP: ARID1A, WB: TAZ. (I) Co-IP of endogenous ARID1A and TAZ in A2780 cells. IP: ARID1A, WB: TAZ. (J) Co-immunoprecipitation of endogenous ARID1A and TAZ in A2780 cells. IP: TAZ, WB: ARID1A. $^{**}P<0.01$ (n=3). ARID1A, AT-rich binding domain 1A; RT-qPCR, reverse transcription-quantitative PCR; TAZ, transcriptional co-activator with PDZ-binding motif; IP, immunoprecipitation; WB, western blotting.

were heavier than the ARID1A-OCSCs group (Fig. 5P). Ki67 staining was then performed to investigate the proliferation of ARID1A-OCSCs xenografts. The present results demonstrated that ARID1A overexpression in OCSC-derived xenografts led to a significant decrease in the proliferation of tumor cells compared with that in the control OCSC-derived xenografts (Fig. 5Q). Thus, ARID1A was shown to inhibit stemness in OCSC xenografts.

Discussion

In the present study, using an *in vitro* cell culture model and an *in vivo* xenograft approach, it was found that ARID1A targets the Hippo/TAZ pathway to decrease the stemness of ovarian CSCs.

ARID1A encodes a large subunit (250 kDa) of mammalian SWI/SNF chromatin remodeling complexes. The ARID1A gene is evolutionarily conserved, and mutations in ARID1A have been found in a broad array of tumor types, including ovarian cancer (13). Previous studies have shown that the loss of ARID1A is associated with the oncogenic transformation of ovarian clear cell adenocarcinoma, and decreased ARID1A expression is correlated with the chemoresistance of ovarian cancer cells (29), indicating the key role of ARID1A in ovarian cancer (30). In the present study, it was revealed that ARID1A negatively regulates ovarian cancer cell viability, migration and colony formation, and contributes to the suppression of EMT and stemness in ovarian cancer cells, further demonstrating the important role of ARID1A in the progression of ovarian cancer. Further studies are needed to identify and define the key amino acid sites in ARID1A that regulate ovarian cancer.

Emerging evidence indicates that several cancers are correlated with aberrant levels of YAP, TAZ, and dysregulated Hippo pathway activity (31,32). Hippo signaling is inhibited in numerous tumors; YAP and TAZ translocate into the nucleus to regulate target genes involved in cell proliferation and the control of cell metastasis and stemness (23). Therefore, the Hippo-YAP/TAZ pathway is considered a key mediator in multiple types of cancers. It was previously reported that overexpression of TAZ promotes the proliferation and migration of R182 human epithelial ovarian cancer cells (33) and that overexpression of YAP elevates the malignant behavior of SK-OV-3 and ES-2 ovarian cancer cells. Consistent with this, it was demonstrated that ectopic expression of TAZ enhances EMT and stemness of SK-OV-3 ovarian cancer cells, reinforcing the notion that TAZ participates in ovarian cancer progression (34). While a previous study demonstrated that ARID1A-containing SWI/SNF complex (ARID1A-SWI/SNF) operates as an inhibitor of the pro-oncogenic transcriptional coactivators YAP/TAZ (35), in the present study it was

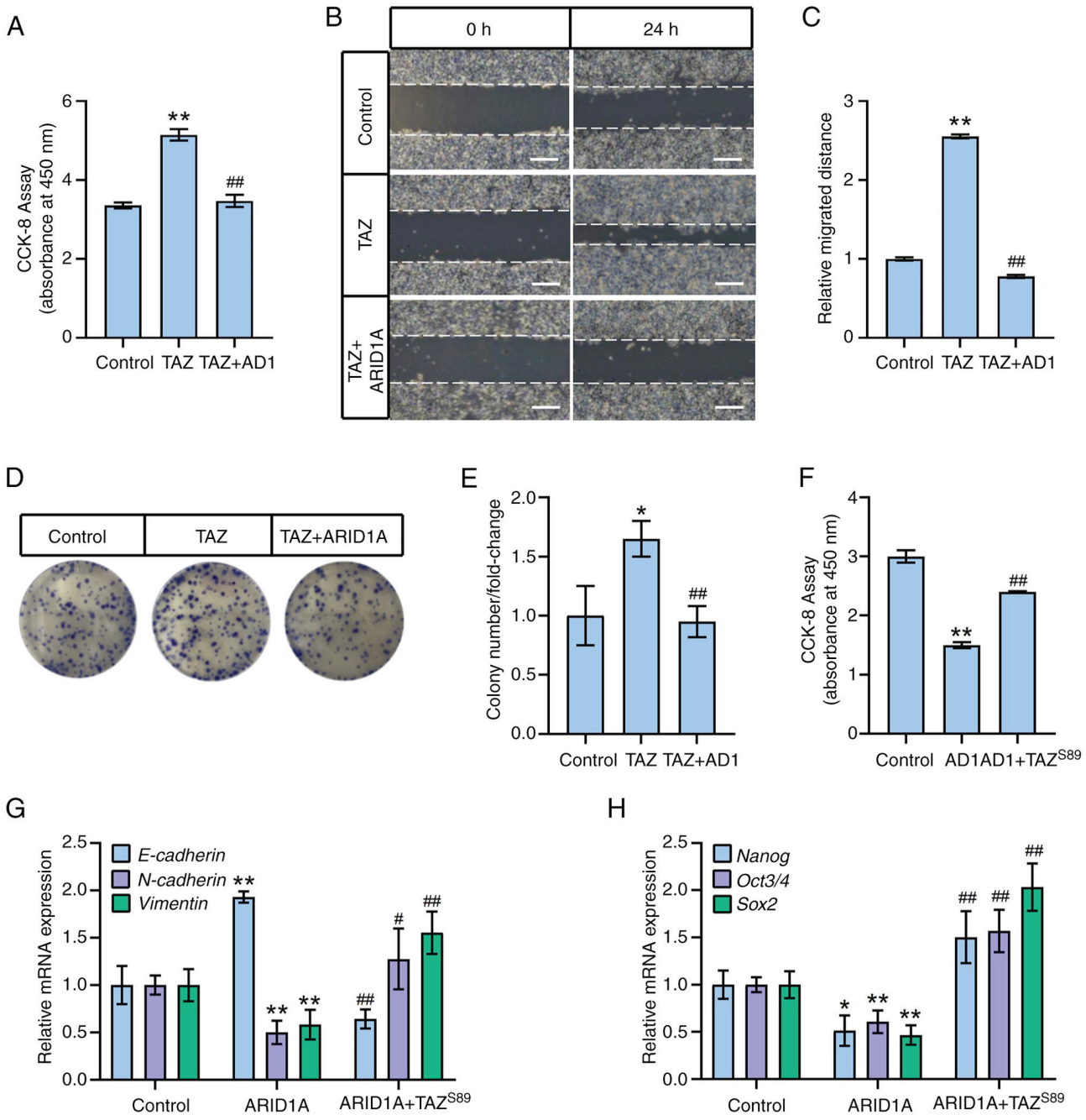

Figure 4. ARID1A inhibits epithelial-mesenchymal transition and stemness through activating the Hippo pathway in ovarian cancer cells. (A) SK-OV-3 cells were transfected with TAZ in combination with ARID1A (AD1) and cell viability was measured after 48 h by CCK-8 assay. (B) SK-OV-3 cells were transfected with TAZ in combination with ARID1A (AD1) and cell migration was measured at 24 h after scratch by wound healing assay. (C) Quantitative statistics of panel B. (D) SK-OV-3 cells were transfected with TAZ in combination with ARID1A and cell colony formation assay was performed. (E) Quantitative statistics of panel D. (F) SK-OV-3 cells were transfected with TAZ-S89-expressing plasmid (TAZ^{S89}) in combination with ARID1A (AD1) and cell viability was measured after 48 h by CCK-8 assay. (G) SK-OV-3 cells were transfected with TAZ-S89-expressing plasmid (TAZ^{S89}) in combination with ARID1A and mRNA levels of E-Cadherin, N-Cadherin and Vimentin were measured by RT-qPCR. (H) SK-OV-3 cells were transfected with TAZ-S89-expressing plasmid (TAZ^{S89}) in combination with ARID1A and mRNA levels of Nanog, Oct3/4 and Sox2 were measured by RT-qPCR. Scale bars in B, 50 μm. *P<0.05 and **P<0.01 vs. Control group; $^{\#}$P<0.05 and $^{\#\#}$P<0.01 vs. TAZ group (A, C, E) or ARID1A group (F-H) (n=3). ARID1A, AT-rich binding domain 1A; TAZ, transcriptional co-activator with PDZ-binding motif; CCK-8, Cell Counting Kit-8; RT-qPCR, reverse transcription-quantitative PCR.

additionally revealed that ARID1A also exerts negative effects on YAP/TAZ-mediated downstream targets by upregulating phosphorylation levels of MST1, an upstream regulator of YAP/TAZ, providing novel linking regarding to ARID1A and Hippo signaling. In addition, the present study it was reported that the altered Hippo activity reciprocally makes a difference in ARID1A expression, further identifying the potential 'cross-talk' between ARID1A and Hippo pathway. Intriguingly, overexpression of a gain-of-function TAZ mutant with a mutation at Ser89 effectively negated the negative regulation caused by ARID1A, indicating that ARID1A-mediated downregulation of cell function in SK-OV-3 cells is dependent on TAZ suppression, which is in contrast to a recently published paper exhibiting that the downregulation of ARID1A promoted

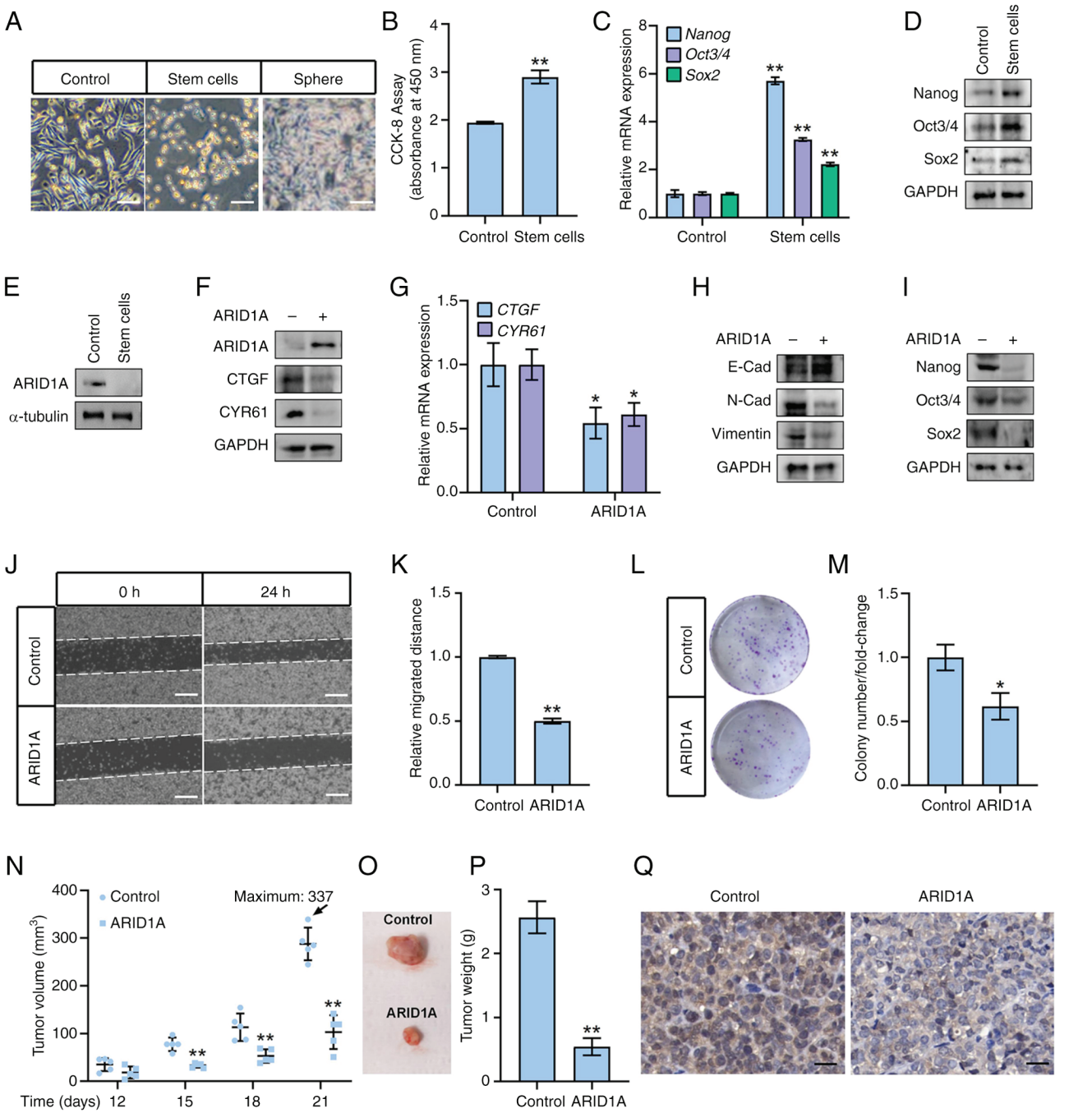

Figure 5. ARID1A-overexpressing OCSCs show less stemness *in vitro* and *in vivo*. (A) Observation with microscope of isolated OCSCs. (B) Viability of OCSCs was measured by CCK-8 assay. (C) mRNA levels of Nanog, Oct3/4 and Sox2 were measured by WB in OCSCs. (D) Protein levels of Nanog, Oct3/4 and Sox2 were measured by WB in OCSCs. GAPDH was used as loading control. (E) Protein levels of ARID1A were measured by WB in OCSCs. α-tubulin was used as loading control. (F) OCSCs were infected with ARID1A-expressing lentiviruses and protein levels of ARID1A, CTGF and CYR61 were measured by WB. GAPDH was used as loading control. (G) OCSCs were infected with ARID1A-expressing lentiviruses and mRNA levels of CTGF and CYR61 were measured by reverse transcription-quantitative PCR. (H) OCSCs were infected with ARID1A-expressing lentiviruses and protein levels of E-Cadherin, N-Cadherin and Vimentin were measured by WB. GAPDH was used as loading control. (I) OCSCs were infected with ARID1A-expressing lentiviruses and protein levels of Nanog, Oct3/4 and Sox2 were measured by WB. GAPDH was used as loading control. (J) OCSCs were infected with ARID1A-expressing lentiviruses and cell migration was measured at 24 h after scratch by wound healing assay. (K) Quantitative statistics of panel J. (L) OCSCs were infected with ARID1A-expressing lentiviruses and cell colony formation assay was performed. (M) Quantitative statistics of panel L. (N) Volumes of xenografts derived from control OCSCs and ARID1A-expressing OCSCs at 12, 15, 18 and 21 days post-inoculation. The maximum tumor volume is indicated. (O) Image showing the size of the representative tumor xenografts from two groups. (P) Weights of xenografts derived from control OCSCs and ARID1A-expressing OCSCs at 21 days post-inoculation. (Q) Ki67 staining for tumor tissues derived from control OCSCs and ARID1A-expressing OCSCs. Scale bars, 100 μm in A, 50 μm in J, 100 μm in P. *P<0.05 and **P<0.01 (n=3). OCSCs, ovarian cancer stem cells; CCK-8, Cell Counting Kit-8; WB, western blotting; ARID1A, AT-rich binding domain 1A.

migration and invasion in human triple-negative breast cancer cells through the Hippo/YAP signaling axis (36), indicating different mechanisms may exist in multiple cancers with particular contexts. Nevertheless, the current data illustrated

at least that TAZ may be a potential novel therapeutic target for the treatment of ovarian cancer, particularly in cases where ARID1A is dysregulated.

Hippo signaling is sensitive to extracellular stimuli such as cell density and mechanical stresses that trigger Hippo activation or inactivation (37). In the past few years, multiple factors have been shown to affect Hippo activity in regulating carcinogenesis, expanding knowledge of the association between the Hippo pathway and tumors. Huang *et al* (38) in 2020 showed that loss of PDLIM1 impedes Hippo signaling to activate YAP in hepatocellular carcinoma. Zhang *et al* (39) in 2019 found that metformin attenuates PD-L1 expression by activating the Hippo signaling pathway in colorectal cancer. In addition, the present study reported that ARID1A modulates the Hippo pathway by regulating the activity of upstream kinases to control ovarian cancer cell function. Given that ARID1A is commonly known as a chromatin remodeling factor and is mainly distributed in the nucleus (15), it would be interesting to understand the molecular mechanisms by which ARID1A regulates the core kinases of the Hippo pathway.

The precise regulation of ARID1A expression is pivotal for maintaining body homeostasis. Dysregulation of ARID1A and mutations in ARID1A are closely associated with various diseases, including cancer (13). It has been found that ARID1A mutation occurs at the early stages of cancer from endometriosis to endometriosis-associated carcinoma in ovarian cancer and also from a typical endometrial hyperplasia to endometrioid adenocarcinoma in endometrial cancer (40). In addition, it was previously identified that ARID1A expression is dramatically decreased and, in some cases, is even lost in ovarian cancer tissues (41-43), indicating ARID1A deficiency has potential as a biomarker for precision medicine of ovarian cancer in clinical settings. In the present study, it was found that activation of the Hippo pathway resulted in a noticeable increase in ARID1A protein expression, whereas overexpression of TAZ-S89 had the opposite effect, which also suggests frequent aberrant ARID1A expression in ovarian cancer cells. Considering that TAZ affects ARID1A protein expression rather than mRNA levels and that TAZ binds with ARID1A, it is worth investigating how TAZ regulates ARID1A protein, and determining whether TAZ-ARID1A protein-protein binding is essential for ARID1A expression alteration. Nevertheless, in addition to the present data, considering the complexity of cancer biology, ARID1A might also regulate EMT and stemness in ovarian cancer through other cell pathways, functioning synergistically with other molecules/genes in ovarian cancer progression, which is worthy of further investigation. Moreover, it is worth verifying the results presented herein in clinical ovarian cancer tissue samples in future, which would provide new target for drug development of ovarian cancer therapy.

In conclusion, developing novel ARID1A-specific agonists may be very effective against ovarian cancer initiation, metastasis and relapse by activating the Hippo/TAZ pathway and attenuating the stemness of ovarian cancer cells.

Acknowledgements

Not applicable.

Funding

The present study was supported by the Starting Research Foundation of The Children's Hospital, Zhejiang University School of Medicine (grant no. 481), the Foundation for The Top-Notch Youth Talent Cultivation Project of Independent Design Project of National Clinical Research Center for Child Health (grant no. Q21A0006), the National Natural Science Foundation of China (grant no. 31801207) to Chao Tang and the National Natural Science Foundation of China (grant no. 32100560).

Availability of data and materials

The data generated in the present study are included in the figures and/or tables of this article.

Authors' contributions

ShoX performed all the experiments and prepared the figures. CZ, QX, ZA and ShuX analyzed the data. GX and CL contributed to the acquisition of data. CT designed the study and wrote the manuscript. All authors read and approved the final manuscript. ShoX and CT confirm the authenticity of all the raw data.

Ethics approval and consent to participate

Animal experiments were approved (approval no. 21045) by the Animal Ethics Committee of Zhejiang University (Zhejiang, China) and performed according to the Guide for the Care and Use of Laboratory Animals (NIH Publication no. 85-23, revised 1996).

Patient consent for publication

Not applicable.

Competing interests

The authors declare that they have no competing interests.

References

1. Webb PM and Jordan SJ: Epidemiology of epithelial ovarian cancer. Best Pract Res Clin Obstet Gynaecol 41: 3-14, 2017.
2. Kurman RJ and Shih IeM: The dualistic model of ovarian carcinogenesis: Revisited, revised, and expanded. Am J Pathol 186: 733-747, 2016.
3. Alsop K, Fereday S, Meldrum C, deFazio A, Emmanuel C, George J, Dobrovic A, Birrer MJ, Webb PM, Stewart C, *et al*: BRCA mutation frequency and patterns of treatment response in BRCA mutation-positive women with ovarian cancer: A report from the Australian Ovarian Cancer Study Group. J Clin Oncol 30: 2654-2663, 2012.
4. Gadducci A, Guarneri V, Peccatori FA, Ronzino G, Scandurra G, Zamagni C, Zola P and Salutari V: Current strategies for the targeted treatment of high-grade serous epithelial ovarian cancer and relevance of BRCA mutational status. J Ovarian Res 12: 9, 2019.
5. Beck B and Blanpain C: Unravelling cancer stem cell potential. Nat Rev Cancer 13: 727-738, 2013.
6. Colak S and Medema JP: Cancer stem cells-important players in tumor therapy resistance. FEBS J 281:. 4779-4791, 2014.

7. Munoz-Galvan S, Felipe-Abrio B, Verdugo-Sivianes EM, Perez M, Jiménez-García MP, Suarez-Martinez E, Estevez-Garcia P and Carnero A: Downregulation of MYPT1 increases tumor resistance in ovarian cancer by targeting the Hippo pathway and increasing the stemness. Mol Cancer 19: 7, 2020.
8. Hu L, McArthur C and Jaffe RB: Ovarian cancer stem-like side-population cells are tumourigenic and chemoresistant. Br J Cancer 102: 1276-1283, 2010.
9. Lee SY, Jeong EK, Ju MK, Jeon HM, Kim MY, Kim CH, Park HG, Han SI and Kang HS: Induction of metastasis, cancer stem cell phenotype, and oncogenic metabolism in cancer cells by ionizing radiation. Mol Cancer 16: 10, 2017.
10. Zhou P, Li B, Liu F, Zhang M, Wang Q, Liu Y, Yao Y and Li D: The epithelial to mesenchymal transition (EMT) and cancer stem cells: Implication for treatment resistance in pancreatic cancer. Mol Cancer 16: 52, 2017.
11. Zheng Y and Pan D: The hippo signaling pathway in development and disease. Dev Cell 50: 264-282, 2019.
12. Tang C, Wang J, Yao M, Ji X, Shi W, Xu C, Zeng LH and Wu X: Hippo signaling activates hedgehog signaling by Taz-driven Gli3 processing. Cell Regen 12: 3, 2023.
13. Xu S and Tang C: The Role of ARID1A in Tumors: Tumor initiation or tumor suppression? Front Oncol 11: 745187, 2021.
14. Mathur R: ARID1A loss in cancer: Towards a mechanistic understanding. Pharmacol Ther 190: 15-23, 2018.
15. Jin M, Xu S, Li J, Li L and Tang C: Role of ARID1A in the regulation of human trophoblast migration and invasion. Reprod Sci 29: 2363-2373, 2022.
16. Yang Z, Li C, Fan Z, Liu H, Zhang X, Cai Z, Xu L, Luo J, Huang Y, He L, *et al*: Single-cell Sequencing Reveals Variants in ARID1A, GPRC5A and MLL2 Driving Self-renewal of human bladder cancer stem cells. Eur Urol 71: 8-12, 2017.
17. Ding DC, Liu HW and Chu TY: Interleukin-6 from ovarian mesenchymal stem cells promotes proliferation, sphere and colony formation and tumorigenesis of an ovarian cancer cell line SKOV3. J Cancer 7: 1815-1823, 2016.
18. Zhu H, Ren Q, Yan Z, Xu S, Luo J, Wu X and Tang C: Human HAND1 inhibits the conversion of cholesterol to steroids in trophoblasts. J Genet Genomics 49: 350-363, 2022.
19. Zhang LL, Xu YL, Tang ZH, Xu XH, Chen X, Li T, Ding CY, Huang MQ, Chen XP, Wang YT, *et al*: Effects of alisol B 23-acetate on ovarian cancer cells: G1 phase cell cycle arrest, apoptosis, migration and invasion inhibition. Phytomedicine 23: 800-809, 2016.
20. Lai D, Wang F, Chen Y, Wang C, Liu S, Lu B, Ge X and Guo L: Human ovarian cancer stem-like cells can be efficiently killed by γδ T lymphocytes. Cancer Immunol Immunother 61: 979-989, 2012.
21. Tang C, Jin M, Ma B, Cao B, Lin C, Xu S, Li J and Xu Q: RGS2 promotes estradiol biosynthesis by trophoblasts during human pregnancy. Exp Mol Med 55: 240-252, 2023.
22. Tang C, Takahashi-Kanemitsu A, Kikuchi I, Ben C and Hatakeyama M: Transcriptional Co-activator Functions of YAP and TAZ Are inversely regulated by tyrosine phosphorylation status of parafibromin. iScience 1: 1-15, 2018.
23. Livak KJ and Schmittgen TD: Analysis of relative gene expression data using real-time quantitative PCR and the 2(-Delta Delta C(T)) Method. Methods 25: 402-408, 2001.
24. Jin M, Cao B, Lin C, Li J, Xu Q, Ren Q, Xu S and Tang C: Tianma gouteng decoction exerts pregnancy-protective effects against preeclampsia via regulation of oxidative stress and NO Signaling. Front Pharmacol 13: 849074, 2022.
25. Akrida I, Bravou V and Papadaki H: The deadly cross-talk between Hippo pathway and epithelial-mesenchymal transition (EMT) in cancer. Mol Biol Rep 49: 10065-10076, 2022.
26. Fu M, Hu Y, Lan T, Guan KL, Luo T and Luo M: The Hippo signalling pathway and its implications in human health and diseases. Signal Transduct Target Ther 7: 376, 2022.
27. Wang J, Liu S, Heallen T and Martin JF: The Hippo pathway in the heart: Pivotal roles in development, disease, and regeneration. Nat Rev Cardiol 15: 672-684, 2018.
28. Liu Q, Stel WV, Noord VEV, Leegwater H, Coban B, Elbertse K, Pruijs JTM, Béquignon OJM, Westen GV, Dévédec SEL and Danen EHJ: Hypoxia Triggers TAZ Phosphorylation in Basal A Triple Negative Breast Cancer Cells. Int J Mol Sci 23: 10119, 2022.
29. Yokoyama Y, Matsushita Y, Shigeto T, Futagami M and Mizunuma H: Decreased ARID1A expression is correlated with chemoresistance in epithelial ovarian cancer. J Gynecol Oncol 25: 58-63, 2014.
30. De P and Dey N: Mutation-Driven Signals of ARID1A and PI3K pathways in ovarian carcinomas: Alteration is an opportunity. Int J Mol Sci 20: 5732, 2019.
31. Dey A, Varelas X and Guan KL: Targeting the Hippo pathway in cancer, fibrosis, wound healing and regenerative medicine. Nat Rev Drug Discov 19: 480-494, 2020.
32. Cunningham R and Hansen CG: The Hippo pathway in cancer: YAP/TAZ and TEAD as therapeutic targets in cancer. Clin Sci (Lond) 136: 197-222, 2022.
33. Jeong GO, Shin SH, Seo EJ, Kwon YW, Heo SC, Kim KH, Yoon MS, Suh DS and Kim JH: TAZ mediates lysophosphatidic acid-induced migration and proliferation of epithelial ovarian cancer cells. Cell Physiol Biochem 32: 253-263, 2013.
34. Wei X, Jia Y, Lou H, Ma J, Huang Q, Meng Y, Sun C, Yang Z, Li X, Xu S, *et al*: Targeting YAP suppresses ovarian cancer progression through regulation of the PI3K/Akt/mTOR pathway. Oncol Rep 42: 2768-2776, 2019.
35. Chang L, Azzolin L, Di Biagio D, Zanconato F, Battilana G, Lucon Xiccato R, Aragona M, Giulitti S, Panciera T, Gandin A, *et al*: The SWI/SNF complex is a mechanoregulated inhibitor of YAP and TAZ. Nature 563: 265-269, 2018.
36. Wang Y, Chen X, Qiao X, Xie Y, Guo D, Li B, Cao J, Tao Z and Hu X: Chromatin Remodelling Molecule ARID1A determines metastatic heterogeneity in triple-negative breast cancer by competitively binding to YAP. Cancers (Basel) 15: 2447, 2023.
37. Ma S, Meng Z, Chen R and Guan KL: The hippo pathway: Biology and pathophysiology. Annu Rev Biochem 88: 577-604, 2019.
38. Huang Z, Zhou JK, Wang K, Chen H, Qin S, Liu J, Luo M, Chen Y, Jiang J, Zhou L, *et al*: PDLIM1 inhibits tumor metastasis through activating hippo signaling in hepatocellular carcinoma. Hepatology 71: 1643-1659, 2020.
39. Zhang JJ, Zhang QS, Li ZQ, Zhou JW and Du J: Metformin attenuates PD-L1 expression through activating Hippo signaling pathway in colorectal cancer cells. Am J Transl Res 11: 6965-6976, 2019.
40. Takeda T, Banno K, Okawa R, Yanokura M, Iijima M, Irie-Kunitomi H, Nakamura K, Iida M, Adachi M, Umene K, *et al*: ARID1A gene mutation in ovarian and endometrial cancers (Review). Oncol Rep 35: 607-613, 2016.
41. Takahashi K, Takenaka M, Okamoto A, Bowtell DDL and Kohno T: Treatment Strategies for ARID1A-Deficient ovarian clear cell carcinoma. Cancers (Basel) 13: 1769, 2021.
42. Winarto H, Tan MI, Sadikin M and Wanandi SI: ARID1A expression is down-regulated by oxidative stress in endometriosis and endometriosis-associated ovarian cancer. Transl Oncogenomics 9: 1177272716689818, 2017.
43. Kawahara N, Yamada Y and Kobayashi H: CCNE1 is a putative therapeutic target for ARID1A-Mutated ovarian clear cell carcinoma. Int J Mol Sci 22: 5869, 2021.

Copyright © 2024 Xu et al. This work is licensed under a Creative Commons Attribution-NonCommercial-NoDerivatives 4.0 International (CC BY-NC-ND 4.0) License.